An automated solar biomass hybrid dryer in rural communities in Ghana

George Obeng-Akrofi[1], Joseph Oppong Akowuah[1], Gifty Opoku-Agyeman[1], Isaac Nkrumah[1], Michael K. E. Donkor[1], Reuben Y. Tamakloe[1], Francis K. Ampong[1], Maike Waldhoff[2], Tobias Klaus[2], Alexander Olenberg[2], Eugeny Kenig[2], Stefan Krauter[2]

[1] Kwame Nkrumah University of Science and Technology, Kumasi (Ghana)

[2] University of Paderborn, Paderborn (Germany)

Abstract

Computational fluid dynamics (CFD) was used to simulate the drying process of a Solar-Biomass Hybrid Dryer (SBHD). CFD simulations were set up with the software StarCCM+ for investigating the temperature distribution inside a 5-tonne prototype in a rural community in Ghana. The predicted temperature distributions were compared to the experimental data of temperature distribution in the dryer. The simulated results of Levels 1 and 2 within the dryer were 5–15 K higher than the experimental data. This was due to the introduction of cold air at the bottom of the dryer and also, the absence of the effect of the fans in the dryer during the simulation process. The simulated results fit nearly perfect for Layers 3 and 4 in the dryer with a deviation of not more than 5 K. All in all, the predicted simulation agrees with the experimental data. In order to improve drying conditions in the SBHD, it is suggested that the integration of an automated system which will aid in the controlled introduction of hot air at high air flow at the lower levels of the shelves in the dryer would be required.

Keywords: CFD simulation, Solar-biomass hybrid dryer, performance

---

1. Introduction

Crop drying has been proven to be an essential process in the preservation of agricultural products (Mastekbayeva, et al., 1999). Being an old technique used for the preservation of food, drying can reduce postharvest loss associated with crops and also make produce lighter, smaller and easier to handle (Green and Schwarz, 2001).

Major drawbacks with open sun drying method as reported by Madholpa et al. (2002) have led to the introduction of enclosed solar structures for drying purposes. Drying of agricultural produce in enclosed solar structures is an attractive way of reducing both the qualitative and quantitative losses of the traditional open-sun drying (Forson et al., 2007). Studies have shown that solar drying techniques lead to a considerable reduction of the drying time and to a significant improvement of the product quality in terms of color, texture and taste as compared to the traditional open sun drying techniques (Fadhel et at., 2014; Srinivasan and Balusamy, 2015; Ajayi et al., 2017).

Solar dryers have a major downside of being weather dependent leading to longer drying times. This has been one of the factors which are impeding the commercialization of such systems in Ghana (Sekyere et. al., 2016). For reaching short drying times, high drying efficiency and product quality, a continuous drying process is targeted. This is the reason why solar biomass hybrid dryers (SBHD) are introduced for reaching constant drying temperatures and a continuous process. With the operation of an external heat source, like a furnace which runs on biomass, the drying process is independent of weather conditions.

The performance in terms of the temperature distribution in the SBHD systems have been studied based on experimental data with little attention geared towards simulated procedures. Carrying out CFD simulations of drying systems can contribute to better design, management and control of such systems. Such studies can help designers analyse spatial temperature and moisture distribution as well as drying time of drying systems prior to scale-up.

doi:10.18086/swc.2017.26.10 Available at http://proceedings.ises.org

The use of CFD modelling for carrying out simulation of drying systems has been proven to be effective and efficient. Such studies help engineers in analysing the performance of drying systems. This goes a long way in the optimization, control and improvement of drying systems in Ghana.

This paper, therefore, sought to study the performance of a 5-tonne capacity SBHD used for drying maize in Ejura, a farming community in Ghana. It was done by using CFD simulated models to validate experimental results.

2. Materials and methods

2.1. Experimental Setup

The 5-tonne capacity Solar Biomass Hybrid Dryer (Fig. 1) is located at Ejura (7° 23′ 0″ N, 1° 22′ 0″ W). It consists of three main parts; the drying chamber, the backup heat generation system and solar photovoltaic system. The dryer has a length of 13 m, the width is 7.85 m and height of 4.6 m. Inside the drying chamber, the shelves have 4 levels with 36 trays on each level.

Fig. 1. 5tonne capacity dryer located in Ejura

2.2. Data Collection of temperature and relative humidity data

Temperature and relative humidity conditions were determined by the use of Tinytag data loggers. The logging date was on 16th October 2016. The logging interval was set at 10 minutes to cater for weather changes at short intervals. During the determination the drying conditions, 5 loggers were placed at each level, 2 on the left and the right side, as well as in the middle, see Fig. 2. The positions of the sensors are implemented in the simulations, to get the temperature variations.

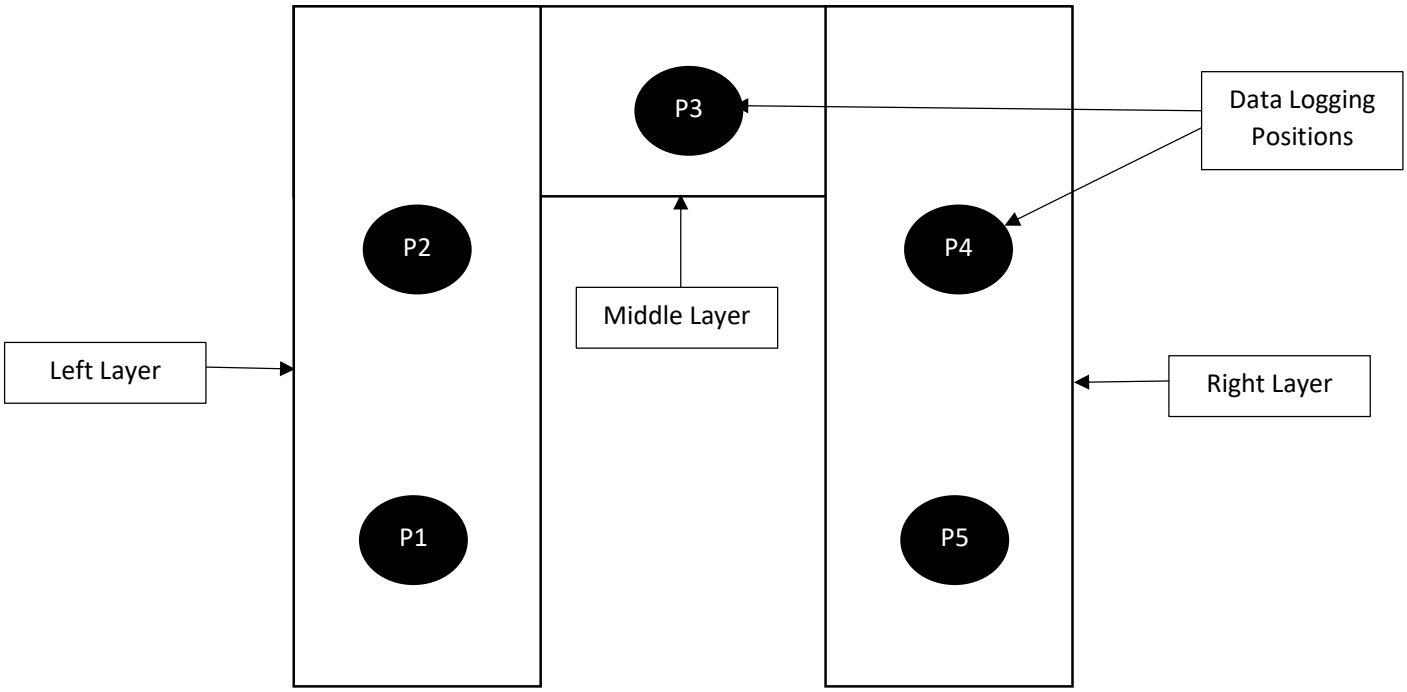

Fig. 2: Layout of shelves and logger positions at each level within the drying chamber

2.3. Physical properties of maize

2.3.1. Heat conductivity and specific heat of maize grain

Heat conductivity and specific heat of maize were determined by Eqn. 1 and Eqn. 2 (Scherer and Kutzbach, 1980; Schwerer and Mühlbauer, 1977)

$$\lambda = 0.108 + (1.80 \times 10^{3} x XM_{H2O}) + (1.79 \times 10^{-4}) \quad \text{(eq. 1)}$$

$$C_{Mp} = 1.294 + (3.44 \times 10^{-2} \times XM_{H2O}) \quad \text{(eq. 2)}$$

Where:

λ is the heat conductivity (W/mK)

XM_{H2O} is the mass water fraction in the maize grain

C_{Mp} is the specific heat capacity of maize (J/ (kg K))

2.3.2. Porosity of maize

The porosity of the maize grains was determined in the laboratory by the use of the water displacement method. Eqn. 3 was used to determine the porosity of the maize grains.

$$\epsilon = \frac{V_V}{V} = 1 - \frac{V_S}{V} \quad \text{(eq. 3)}$$

Where:

V_V is the volume of void

V_S is the volume of solid (maize grains)

V is the total volume of measuring cup

2.3.3. Diameter of maize grain

With the total volume of the maize grains, it was possible to determine the particle volume of a sphere, which is equivalent to the volume of one maize grain. The maize volume was divided by the number of maize grains to get the average volume of one maize grain. The diameter of the maize grain was calculated using Eq. 4.

$$d_p = \sqrt[3]{\frac{6V_g}{\pi}} \quad \text{(Eq. 4)}$$

Where:

d_p is the diameter of a maize grain

V_g is the volume of a maize grain

2.4. Geometry of the SBHD

3D model of the dryer was drawn in the software Autodesk Inventor and exported as a CAD file to StarCCM+ as shown in Fig. 3. In order to set up the simulation, not the original geometry was used, but the geometry in which the fluid flows. The shelves, the maize layers, the inlet, the outlet and the glass are separated in volumes to create single geometry parts for each volume during the import of the CAD file to StarCCM+. Afterwards, a region is created for each geometry part, in order to be able to set individual material properties for each region, e.g. heat conductivity for maize, air and PMMA. The fluid and the porous region are subtracted from the glass shape to get the fluid geometry. Four trays are combined to one maize region to reduce the computational effort, and as a result, each layer is divided into 9 sub-regions.

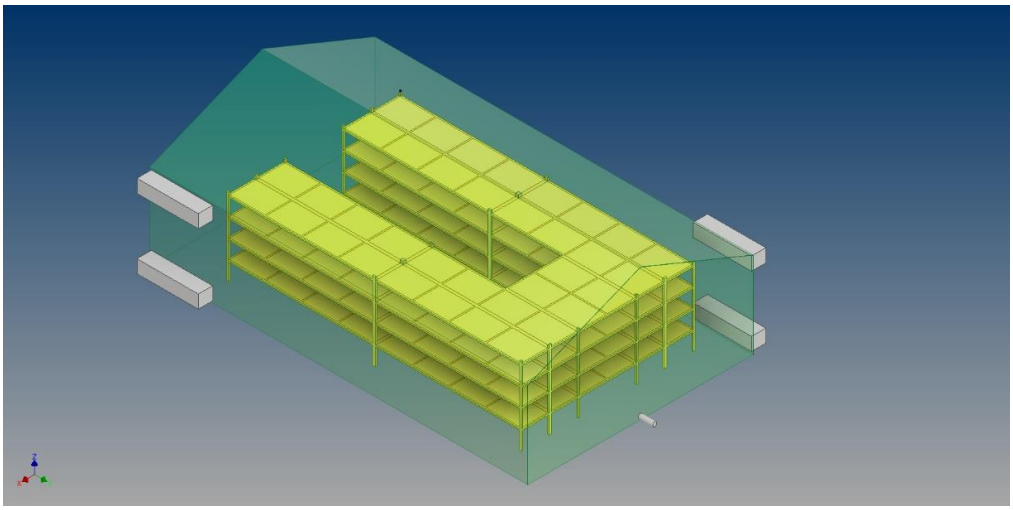

Fig. 3: 3D model of the SBHD

2.5. Boundary conditions

Boundary conditions are set to solve the differential equations. At the pipe, the boundary conditions velocity inlet with 0.25 m/s is defined. Furthermore, the state of the air is given by the data sheets with an average temperature of 305 K and an absolute water mass fraction of 0.025. The relative humidity was transformed into mass fraction xH_2O with Equation 5. The thermodynamic software REFPROP calculates the saturation pressure (REFPROP, 2017).

$$x_{H2O} = \varphi \frac{P_S(t)}{P_M} \quad \text{(Eq. 5)}$$

Where:

P_s is the saturation pressure

P_m is the pressure of the mixture

At the outlet of the drying chamber, a pressure boundary with a relative pressure of 0 Pa is set. The no-slip wall boundary condition is set for the PMMA sheets, the shelve of the maize layers and the floor. For modelling, the solar radiation, the transmissivity, the emissivity and the reflectivity are defined at the interfaces between the fluid and the PMMA region. Table 1 shows the boundary conditions set for the simulation.

Table 1: Boundary conditions for the simulation

Part	**Region**	**Boundary Condition**
input	**fluid**	**velocity inlet**
variable	**value**	**entity**
species mass fraction	0.972, 0.028	-
temperature	0.0006.t +296.88	K
emissivity	0.8	-
reflectivity	0.2	-
transmissivity	0.0	-
velocity	0.25	m/s^2
output	**fluid**	**pressure outlet**
pressure	0	P a
PMMA	**glass**	**wall**
emissivity	0.05	-
reflectivity	0.05	-
transmissivity	0.05	-
heat transfer co-efficient	3	$\frac{W}{m^2K}$

2.6. Simulation Procedure

CFD simulations were set up with the software StarCCM+ for investigating the temperature distribution inside the 5-tonne prototype. Before building up the final simulation, the physical phenomena (radiation, fluid flow, heat transfer and species transfer) which occur in the drying process were described by matching numerical models given by StarCCM+. Most important step in describing the drying process was to find an adequate approach for the heat and species transfer. With this approach, the temperature variations in the maize and drying air were calculated. The geometry, through which the fluid flows, was drawn in the software Autodesk Inventor and imported to StarCCM+. Then the given operating parameters (e.g. temperature, relative humidity and velocity at the inlet) and material properties (e.g. transmissivity for the PMMA, maize density) are implemented. Subsequently, the simulation is carried out and the resulting temperature distribution is compared to measurements to evaluate the used models and boundary conditions.

3. Results and discussion

3.1. Dynamics of fluid flow

The simulation of turbulent flow with velocities between $0\ \frac{m}{s}$ and $1.616\ \frac{m}{s}$ are shown in Fig. 4. As expected, the maximum and minimum velocities are close to the inlet and outlet of the dryer. Between the layers, the velocities decrease between $0.323\ \frac{m}{s}$ and $0.646\ \frac{m}{s}$. The velocities at the top of the dryer are approximately $0\ \frac{m}{s}$.

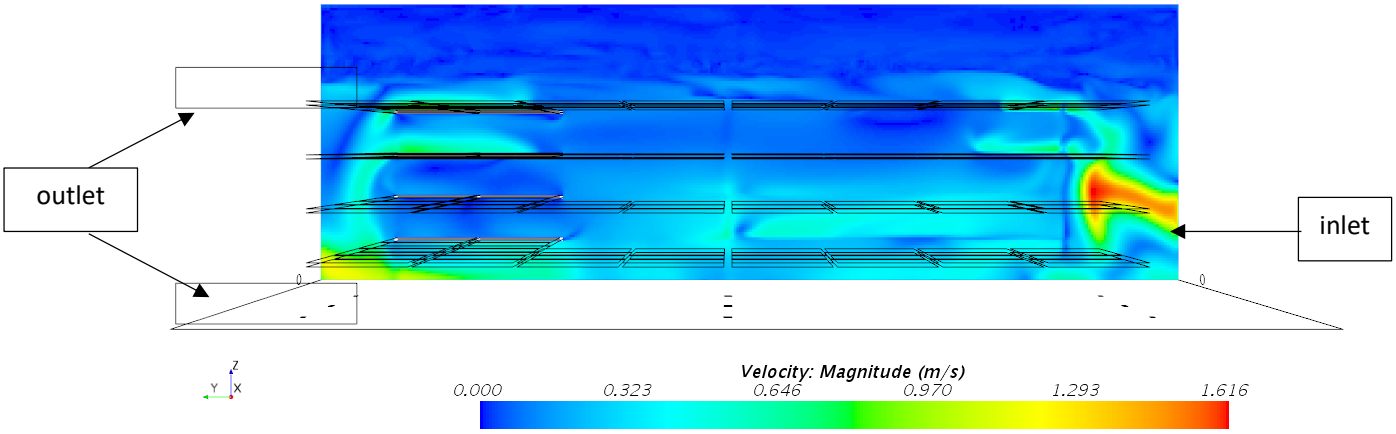

Fig. 4: Velocity field for the unsteady turbulent case

With a closer look at the turbulent viscosity ratio in Fig. 5, the laminar and turbulent flow can be evaluated. The turbulent viscosity ratio between the layers is 600. Hence, the laminar flow cannot be further evaluated, due to the turbulent areas between the layers. With this, the temperature distribution was observed for the turbulent flow.

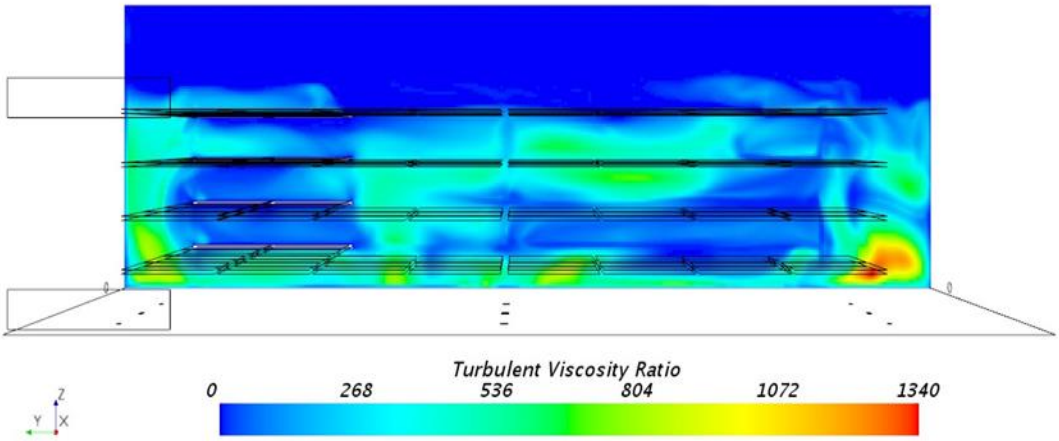

Fig. 5: Scalar Scene for the turbulent viscosity ratio

3.2. Temperature Distribution

Temperature changes are caused by the invading solar radiation and the incoming air; both variables depend on the daytime. The temperature distributions were carried out for a case where the heat transfer coefficient of the Perspex walls was $3\,\frac{W}{m^2K}$. The results for the temperature distribution inside the drying chamber are shown in Fig. 6. Two temperature fronds are developed in Fig. 6. The temperatures close to the roof reached between 340 K and 380 K, and the temperatures around the layers are between 305 K and 330 K. The intruding radiation heats up the drying chamber. This causes hot air to rise due to the density variations, whereas through the pipe at the input, cooler air gets in the drying chamber. The overheating at the top of the drying chamber can result in irregular product quality at the Layer 4 and Layers 1 to 3.

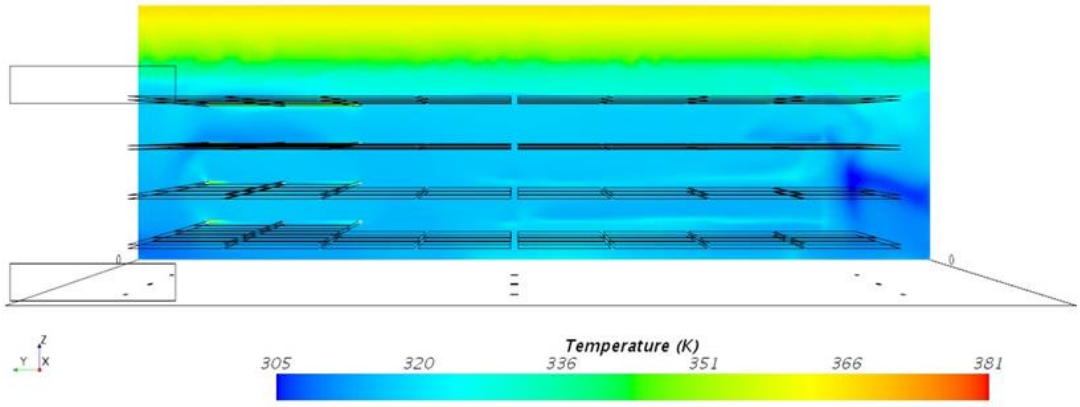

Fig. 6: Scalar Scene for the temperature distribution for the $3\,\frac{W}{m^2K}$ non-adiabatic wall

The simulation results are compared with experimental data to evaluate the simulations. Temperature distributions for Layers 1, 2, 3 and 4 for the non-adiabatic case are displayed in Fig. 7, 8, 9 and 10 respectively. The temperature function of the simulation results was calculated by Excel to get a smooth distribution and are displayed as dotted lines. The continuous lines display the experimental data. The data from sensor P1 and P2 are averaged to S1. Accordingly, P3 and P4 are averaged to S2. The simulation results for the temperature in Layer 1 (Fig. 7) are up to 15 K higher than the experimental data but the variation decreases in Layer 2 up to 5K (Fig. 8). The simulation results fit nearly perfectly in Layer 3 and Layer 4 (shown in Fig. 9 and 10) for the non-adiabatic case. The high temperatures from the simulation was due to the fact that the dryer was drawn as a continuous shape, but the constructed one in Ejura (Fig. 1) is leaking. Furthermore, temperature differences can be explained by changes in weather, whereas StarCCM+ calculates solar radiation without interruptions. Also, higher temperatures in Layer 1 and Layer 2 in the simulation, can be caused by the missing fans which are installed in the dryer but not considered in the simulations.

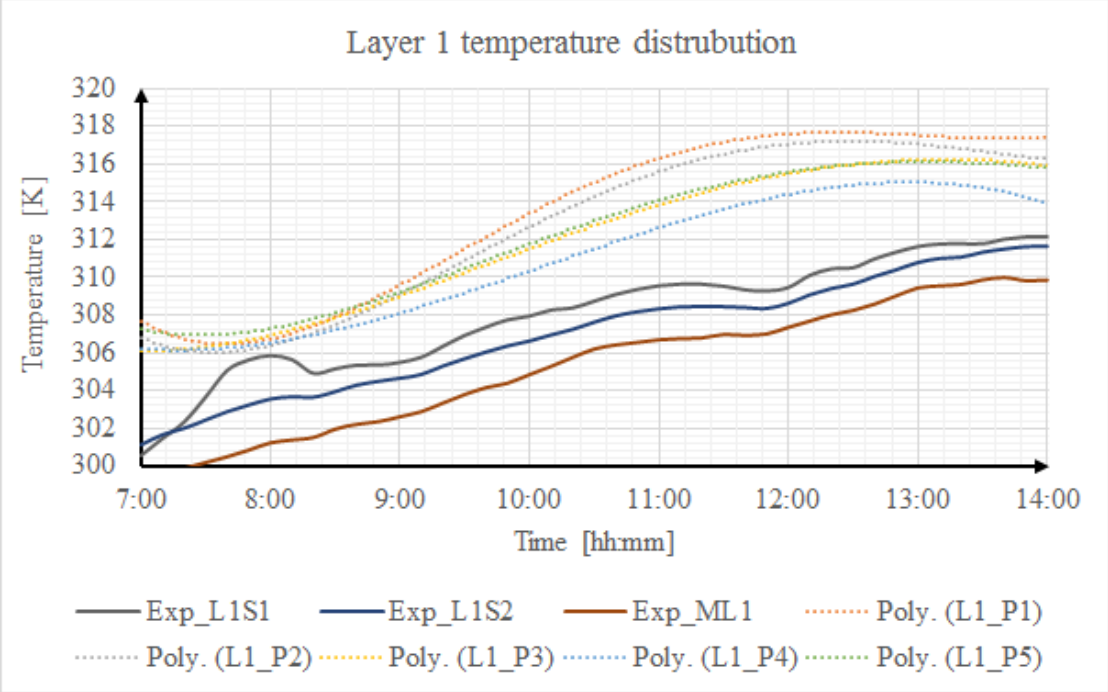

Fig. 7: Temperature distribution for Layer 1

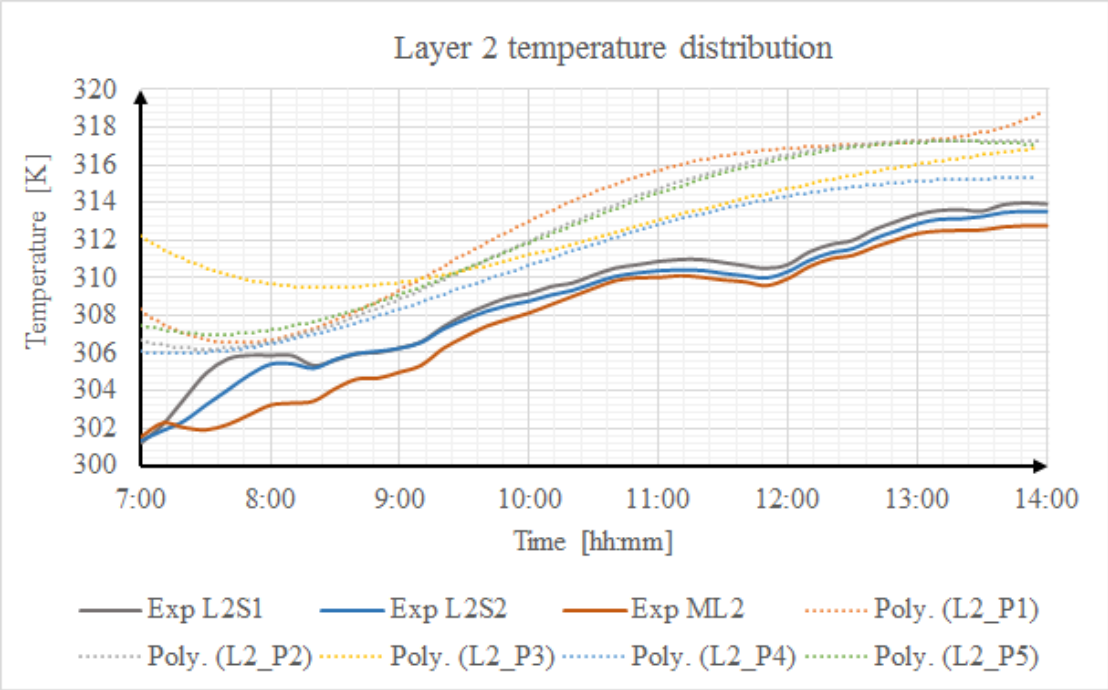

Fig. 8: Temperature distribution for Layer 2

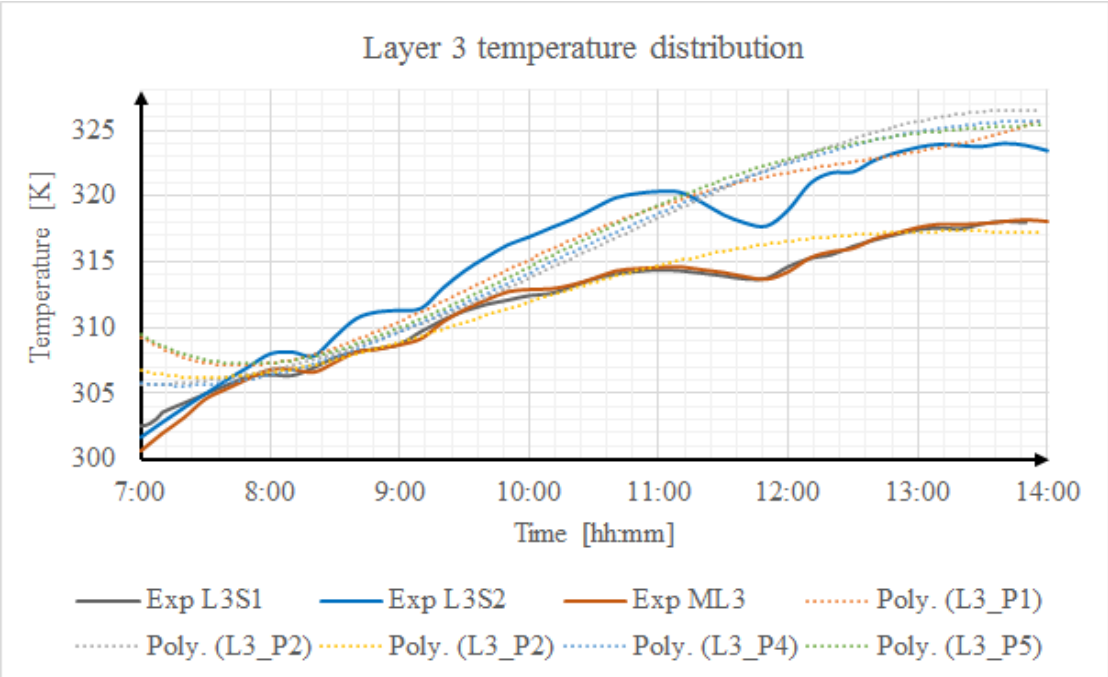

Fig. 9: Temperature distribution for Layer 3

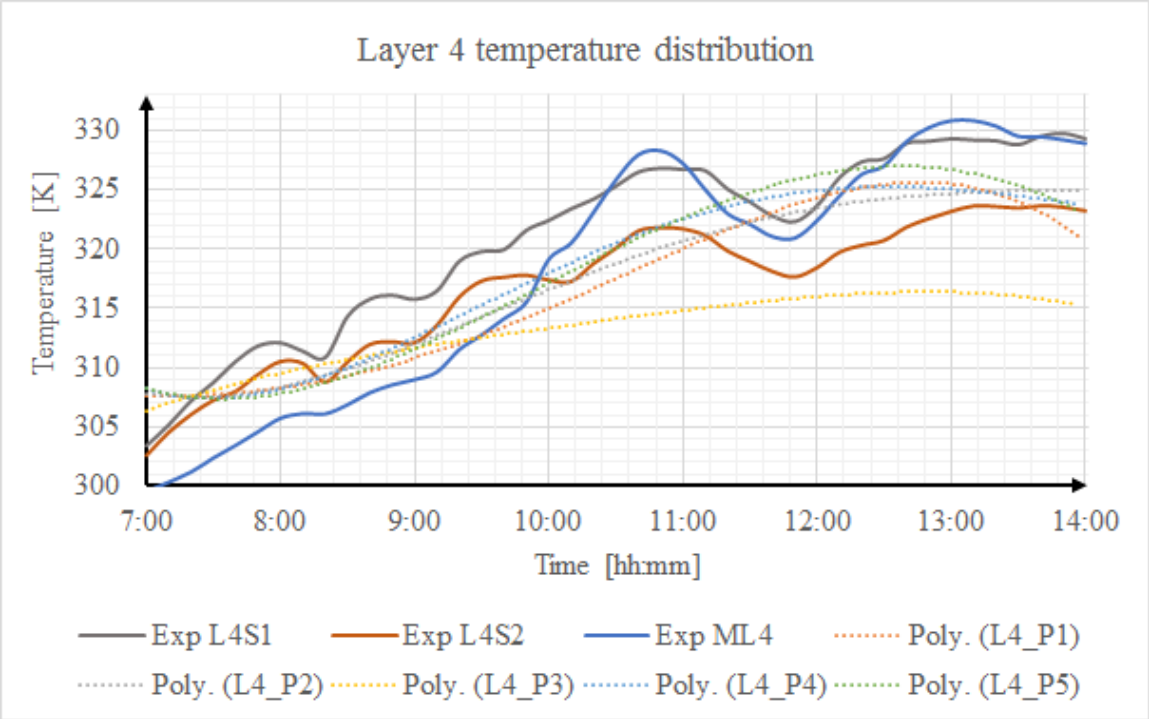

Fig. 10: Temperature distribution for Layer 4

3.3. The automated system

The uneven distribution of temperature in the SBHD could be resolved by the introduction of an automated system. This in addition could also help in the regulation of temperature in the dryer to provide drying conditions which will suit different types of crops.

An electronic circuit consisting of DHT22 temperature and humidity sensors would be designed by the use of Raspberry Pi microcontroller. The Raspberry Pi would be used because of its ability to run Graphic User Interface (GUI) application. The aim of the GUI interface is to enable the users of SBHD to easily interact with the automated system, control and be informed about drying conditions in the dryer. Instead of the conventional keyboard and mouse, an LCD touch screen would be attached to the device to provide a simple interface between the user and the drying system.

Fig. 11 shows the arrangement of the various systems in the automation with the input being the DHT22. The pump and servo motor serve as the outputs of the biomass furnace when the weather and/or drying conditions are not favourable. The DHT22 sensors get signals of temperature and humidity conditions inside the dryer and then relay these signals to the microprocessor. The microprocessor then sends information to the suction pump to either allow or disallow the driving of hot air from the biomass furnace into the dryer. The servo motor acts as the main mechanism to control the movement of shutters at the inlet from the suction pump in to the dryer as shown in Fig. 12. The operations of the suction pump and the servo motor depends on the drying conditions in the dryer. For instance, when temperature in the dryer is lower than the required drying temperature, DHT22 sensor will send signal to the microprocessor for the microprocessor to start the operation of the suction pump.

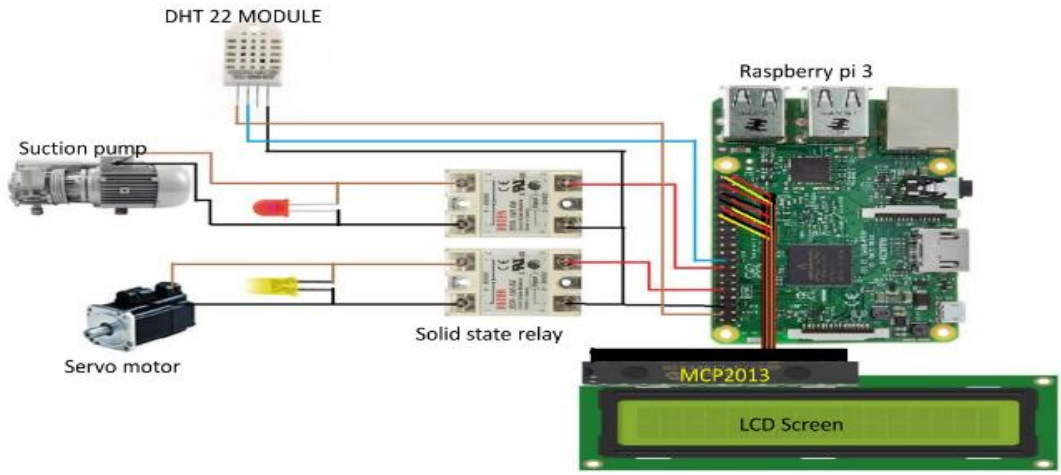

Fig. 11: Schematic circuit of the automated system

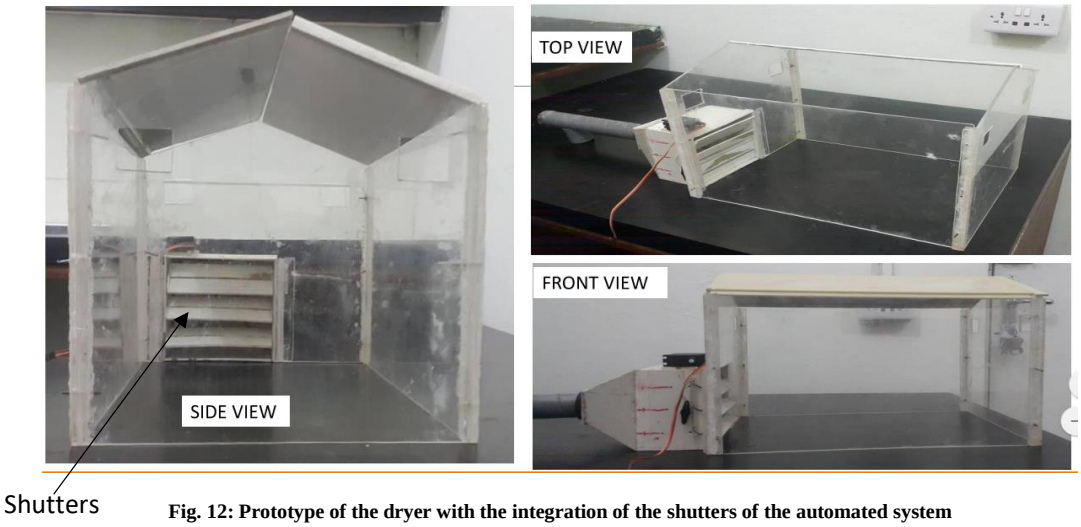

Fig. 12: Prototype of the dryer with the integration of the shutters of the automated system

4. Conclusion

The aim of this work was to develop a CFD model for the Solar Hybrid dryer. The resulting temperature distribution for the heat transfer was compared to experimental data. The comparison showed that the status quo of the dryer was abstracted in a suitable way by the CFD model. Although some deviations between the model and the data exist, they can be explained by the differences between the geometry of the model and the dryer at Ejura. In contrast to the ideal CAD geometry, the physical dryer has several leakages caused by the manufacturing process.

A satisfactory model for describing the status quo of the prototype is compulsory for performing further case studies. For example, case studies can be carried out to investigate the influence of different operation conditions (higher inlet temperature with the furnace, variation of inlet velocities) on the drying process. Furthermore, the dimensions of the shelves (height between the layers, depth of the maize on the layers) can be varied to display effects on the heat and moisture distribution. Again, the integration of an automated system which will aid in the controlled introduction of hot air at high air flow at the lower levels of the shelves in the dryer would help in controlling the temperature of the dryer and then introduce heat from the biomass furnace where weather conditions are not favourable.

5. References

1. Ajayi, O.A., Ola, O.O., Akinwunmi, O.O., 2017. Effect of drying method on nutritional composition, sensory and antimicrobial properties of Ginger (Zinginber officinale). International Food Research Journal, 24(2).
2. Ajayi, O.A., Ola, O.O., Akinwunmi, O.O., 2017. Effect of drying method on nutritional composition, sensory and antimicrobial properties of Ginger (Zinginber officinale). International Food Research Journal, 24(2).
3. Belessiotis V., Delyannis E., 2011. Solar Drying. Solar Energy 85, 1665–1691
4. Fadhel, A., Kooli, S., Farhat, A. and Belghith, A., 2014. Experimental study of the drying of hot red pepper in the open air, under greenhouse and in a solar drier. Int J Renew Energy Biofuels, 2014.
5. Fadhel, A., Kooli, S., Farhat, A., Belghith, A., 2014. Experimental study of the drying of hot red pepper in the open air, under greenhouse and in a solar drier. Int J Renew Energy Biofuels.
6. Forson, F.K., Nazha, M.A.A., Akuffo, F.O., 2007. Design of mixed-mode natural convection solar crop dryers: application of principles and rules of thumb, Renewable Energy 32 - 2306 - 2319.
7. Mastekbayeva, G.A., Bhatta, C.P., Leon, M.A. and Kumar, S., 1999, July. Experimental studies on a hybrid dryer. In ISES 99 Solar World Congress (pp. 4-9).
8. REFPROP accessed on 10th October 2017. <https://www.nist.gov/srd/refprop>
9. Scherer, R, Kutzbach, H.D., 1980. The heat and temperature conductivity of grains. Basic principles of Agricultural Engineering. Vol. 30 No.1:21–27.
10. Schwerer, R., Mühlbauer, W., 1977 The specific heat of grains. Basic principles of Agricultural Engineering. Vol 2 No. 2: 33-40.
11. Sekyere, C.K.K., Forson, F.K., Adam, F.W., 2016. Experimental investigation of the drying characteristics of a mixed mode natural convection solar crop dryer with back up heater. Renewable Energy 92, 532 – 542
12. Srinivasan, R. and Balusamy, T., 2015. Comparative studies on open sun drying and forced type (mixed mode) solar drying of bitter gourd. Journal of Chemical and Pharmaceutical Sciences www. jchps. com ISSN, 974, p.2115.